Arab J. Nucl. Sci. Appl., Vol. 57, 3, 11-23 (2024)

ISSN 1110-0451

Arab Journal of Nuclear Sciences and Applications

Web site: ajnsa.journals.ekb.eg

(E S N S A)

Realizing the advantages of Replacing Lead with Tin in Bismuth-Lead Alloys for Improved Thermal and Nuclear Properties as Coolant

Samah Dahy[1], R.M. El Shazly[2], T.Z.Amer[1], N.S. Gomaa[1], A.A. Bahgat[2*]

(1) Physics Department, Faculty of Science, Al-Azhar University, Girls branch, Nasr City, 11884, Cairo, Egypt

(2) Physics Department, Faculty of Science, Al-Azhar University, Nasr City, 11884, Cairo, Egypt

ARTICLE INFO

Article history:

Received: 5th Apr. 2024

Accepted: 22nd May 2024

Available online: 5th June 2024

Keywords:

Liquid metal coolant;
Wettability;
Melting points;
γ-rays and neutrons absorption;
Mass attenuation coefficients;
Build-up factors;
and Neutrons macroscopic cross-sections.

ABSTRACT

A series of $Bi_{50}Pb_{50-x}Sn_x$ alloys, where x = 0, 16, 20, 25, and 30 wt. %, were prepared to be used as coolants and for heat transfer in fast fission and/or fusion nuclear reactors. For the prepared alloys, measurements were made of their density and melting points. Similarly, high-temperature measurements of the alloys' wetting contact angles on several substrate types were made to clarify their possible application in the design of nuclear reactors. The mass attenuation coefficients μ_m (cm^2/g) were established experimentally with energy ranges of 121.8 to 1407.24 keV. The neutron macroscopic cross sections Σ (cm^{-1}) and mean free path MFP (cm) of the alloys were determined experimentally using three neutron energy ranges (slow neutrons, total slow neutrons, and neutrons with energies > 0.4 eV). The results indicated that there was a substantial agreement between the theoretical calculations which were done with the aid of "WinXCom" and "Phy-X/PSD" software and the practical outcomes. The increase in Sn concentration at the expense of Pb improves the physical characteristics of (Bi-Pb-Sn) alloys, making them suitable for use as coolants in fast nuclear reactors.

1. INTRODUCTION

Liquid metals have been employed in different systems for generating energy because of their excellent thermal qualities, particularly their low point of melting and high boiling temperatures [1]. Additionally, their neutronic characteristics are therefore particularly appealing for fission and/or fusion nuclear reactors and the nuclear generation's system [2]. Recently, liquid metals are being employed in a variety of applications, including cooling computer chips [3], in neutron spallation, in which the heavy metals are targeted by protons with high energy for producing high-intensity neutron fluxes [4]. Furthermore, in a potential nuclear application, they could be employed as coolants for nuclear fusion reactors [5] to transfer heat created by particle bombardment [6] and in solar power generation installations [7] a high temperature lubricant [8], and as a soldering and brazing materials.

Lead and bismuth eutectic (LBE) are being considered potential coolants for the next generation of fast nuclear reactors (critical and subcritical), which will have a very high level of self-protection and safety against serious accidents [9]. Initially, sodium was chosen as the primary coolant for the fast reactor because of its superior heat transfer ability. However, sodium has significant drawbacks as a coolant, including a high chemical reaction with water that produces extreme heat, which could cause a huge explosion, in addition to its performance in chemical corrosion [10].

Nuclear reactor designers are increasingly focusing on lead and LBE cooling systems. Liquid LBE is used for heat transfer in nuclear reactors due to its thermophysical and nuclear properties [11]. J.R. Weeks [12] suggested liquid tin (Sn) for nuclear power stations and considered melts of natural Sn as coolant for fast-nuclear reactors due to the appealing properties of tin. Qian et al [13] investigated the idea of replacing liquid sodium with liquid tin in the coolant system to enhance the reactor safety features, whereby the proportion of delayed neutrons in the core of a reactor with liquid tin can be raised by doping a small quantity of Pu and diluted U. This is difficult when using liquid sodium due to its reactivity. Toshinsky et al. [14] alternatively, examined the attractive qualities of LBE and lead as coolants for fast nuclear reactors, which would have a very high level of

Corresponding author: alaabahgat@hotmail.com

DOI: 10.21608/AJNSA.2024.281619.1809

protection. While Amer et al. [15] undertook a practical comparison of the physical properties of both (Pb–Bi–Cd) alloys and LBE, they showed that the physical properties of (Pb-Bi-Cd) alloys would be suitable for use as a coolant in a fast nuclear reactor. Moreover, Dahy, et al. [16] investigated the thermal and nuclear properties of (Bi–Pb) alloy and (Bi–Pb–Sn–Cd) alloys, concluding that the (Bi–Pb–Sn–Cd) alloys would be adequate for use as a coolant in fast nuclear reactors and as outer cooling blanket containers, despite the presence of Cd-metal which has a minimal effect on fast neutrons.

Generally, bulk density is one of the most important factors to consider when selecting the type of reactor coolant. This is because high-density coolants complicate reactor design and need higher pumping power to circulate the coolant. Using liquid coolant can be advantageous for certain purposes, but it also has some drawbacks that need to be considered. One of these drawbacks is the high density of the coolant, which is especially true for LBE. Its density is almost ten times greater than that of sodium liquid, making it more challenging to pump. In fact, pumping LBE requires 6-7 times greater power than pumping Na. With this in mind, it's worth considering the benefits of using liquid coolant against the additional power requirements necessary to pump it, to determine if it's the right choice for our specific needs [17]. Additionally, the LBE contains a high percentage of lead, which belongs to the heavy metal toxin, which is harmful to the health and environment. While it has a low melting point, it can be used at suitable temperatures without the risk of freezing or boiling uncontrollably.

On the other hand, tin metal, Sn, has attractive thermal properties; it has a high boiling point (2270 °C) as well as a low melting point (232 °C) compared to Pb (327.4 °C) and Bi (271.41 °C), Also, the density of Sn is less than that of Pb (ρ_{Sn}= *7.31 g/cm*^{3}, ρ_{Pb}=*11.35 g/cm*^{3}). While, it offers very high heat removal ability, up to 1 GW/m^3 at temperatures between (400-600 °C) [17].Therefore, in the present work, alloys of bismuth-lead-tin, substituting lead by discrete weight percentages of tin metal, were proposed and prepared to study the effect of substitution of Sn metal at the expense of Pb in the (Bi-Pb) alloy on their physical properties and explore the possibility of utilizing them as coolants and for heat transfer in fast fission and/or fusion nuclear reactors.

2. EXPERIMENTAL TECHNIQUES

The experimental and analytical work presented next was conducted exclusively with the facilities available in the Physics department through local efforts.

2.1 Preparation of samples

Table 1 shows the various liquid metal alloys that were prepared from bismuth, lead, and tin with a purity of 99.99 %. Alloys were prepared by melting in a Pyrex tube on a benzene flame; to avoid oxidation by air throughout the melting process, the components were covered with 1.0 wt. % allophonic acid ($C_2H_4N_2O_3$). The components were heated for about 15 minutes, shaking the tube to achieve homogeneity in the melt. Following melting, the tube was broken to produce the alloy. To remove the excess allophonic acid, the alloy was immersed in pure carbon tetrachloride (CCl_4) for three minutes [18].

Table (1): Composition of the prepared alloys.

Sample	Bi wt-%	Pb wt-%	Sn wt-%
BL	50	50	-
BLSn1	50	34	16
BLSn2	50	30	20
BLSn3	50	25	25
BLSn4	50	20	30

2.2 Bulk density and molar volume

The displacement method, with carbon tetrachloride (CCl_4), was utilized to evaluate density of prepared alloys using the equation [19];

$$\rho_{Exp} = \frac{W_{air}}{W_{air}-W_{liquid}} \times \rho_{liquid} \quad \textbf{(1)}$$

Where W_{air} and W_{liquid} represent the weights in air and liquid, respectively; ρ_{Exp} and ρ_{liquid} is the density of the sample and liquid, respectively. On the other hand, the theoretical density was determined using the equation [16];

$$\rho_{Cal} = \sum_{i=1}^{N} wt_i \rho_i \quad \textbf{(2)}$$

Where, $wt_i\%$ is the weight percentage and ρ_i is the densities of the alloy elements. The porosity percentiles for the prepared alloys were estimated using the equation. [16];

$$porosity\ \% = 1 - \frac{\rho_{Exp}}{\rho_{Cal}} \quad \textbf{(3)}$$

The molar volume V_m of the produced alloy was estimated using the formula [20];

$$V_m = \sum_{i=1}^{N} \left(\frac{x_i M_i}{\rho_{exp}}\right) \quad \textbf{(4)}$$

Where x_i and M_i are a molecular percent and the weight in mole of *i-th* molecule, respectively; ρ_{exp} is the measured density expressed in *g.cm*$^{-3}$.

2.3 Differential thermal analysis (DTA) Technique

The melting temperature of the present specimens was determined using a homemade, well calibrated differential thermal analyzer (DTA) [19]. The collected data was analyzed using the Origin program, version 8.5. The current technique measures the temperature difference (ΔT) between the sample and reference (Al_2O_3) with time and temperature recorded. The heating rate was set to 14.0 ºK/min across all samples. Melting points (T_m) were established at the low-temperature edge of the endothermic peak, which exist in a ±1.5 ºK error.

2.4 Wettability measurements

The wettability of liquid metals with solid materials is extremely important in industrial applications such as metal forming, welding, bonding structural ceramics, stabilizing metal and ceramics, and removing solid impurities from molten metals, among others [21]. In addition, wettability is critical to the choice of pipes transporting the coolant around the reactor core, as well as the materials used in the reactor chamber and vessel.

Contact angle, CA, namely θ, is one of the methods used to measure the wettability of a surface or substance, If $\theta < 90^0$ it indicates that the solid is wet by the liquid; If the contact angle is equal to 90 degrees, it is intermediate-wet; otherwise, if $\theta > 90°$ it designates that the solid is non-wetting by the liquid; if $\theta = 0$, it indicates that the solid is completely wetted by the liquid; and if $\theta = 180°$ it indicates that the solid is completely non-wetting by the liquid [22].

A liquid drop's CA on an ideal solid substrate is determined by its mechanical equilibrium under the influence of three interfacial tensions:

$$\gamma_{lv} \cdot cos\ \theta_Y = \gamma_{Sv} - \gamma_{sl} \qquad \textbf{(5)}$$

Where θ_Y represents Young's contact angle, γ_{lv}, is the liquid-vapor interfacial tension, γ_{sv}, is the solid-vapor interfacial tension, and γ_{sl} is the solid-liquid interfacial tension [23].

The CA of prepared alloys was evaluated photographically on different metals substrate: steel-37 (St-37) and aluminum (Al). For adjusting the image scales and improving the appearance, a reference stainless steel sphere was utilized. The photograph was collected every 10 seconds at elevated temperatures until it reached a steady state. The Auto Cad computer program was used to evaluate the contact angle.

2.5 Nuclear measurements

Generally, the absorption and attenuation of gamma rays [24] and neutrons [25] depend on the bulk density of the substance under study. At 293.1 ºK, for example the density of the Pb–Bi eutectic solid alloy phase is 10.705 g/cm^3, and it drops to 10.5228 g/cm^3 in the liquid phase at 400 ºK, a decrease of about 1.70 % according to ref. [26]. Consequently, in the temperature range considered in our present studies, we can accept the measurements of absorption data at room temperature at the solid-state phase as adequate, which should reflect the corresponding performance of the liquid phase at a temperature above 400 ºK.

2.5.1 Gamma-Rays Attenuation

Three gamma-ray sources; Co-60, Cs-137, and Eu-152 were utilized to study gamma-ray attenuation for the prepared alloys using a 3\\ x 3\\ NaI (Tl) scintillation detector. The attenuation coefficients were determined at nine distinct photo peaks (121.8, 344.27, 661.64, 778.9, 964, 1112.4, 1173.23, 1332.5, and 1407.24 keV) to include a wide range of energies. The linear attenuation coefficient (μ, cm^{-1}) of the prepared alloys was evaluated using the Beer-Lambert equation [27]:

$$I_x = I_0 e^{-\mu x} \qquad \textbf{(6)}$$

Where I_o and I_x are the incident and transmitted intensities, respectively, and x is the alloy thickness. The half-value layer (*HVL*,*cm*) was estimated to determine the material thickness needed to reduce the intensity of gamma rays to half its initial intensity. The *HVL* was calculated by using the following equation [27]:

$$HVL = \frac{ln2}{\mu} \qquad \textbf{(7)}$$

To ensure that the state of the material (solid, liquid, or gases) does not affect the attenuation coefficients, the value of the mass attenuation coefficient *MAC* (μ_m, cm^2/g) [27] was considered and evaluated using the following equation:

$$\mu_m = \frac{ln\ (\frac{I_0}{I_x})}{x\rho} \qquad \textbf{(8)}$$

Where ρ represent the alloy bulk density. In addition to the experimental results, the online windows version of the X-Com program "WinXCom" (version 3.1) [28] was employed to determine *MAC* (μ_m, cm^2/g) by using the following equation:

$$\mu_m = \sum_i^n w_i \left(\frac{\mu_i}{\rho_i}\right)_m \qquad \textbf{(9)}$$

Where $\left(\frac{\mu_i}{\rho_i}\right)_m$ is th *MAC* for each individual element in the alloy, and w_i is the fractional weight of the constituents of each alloy [29]. Correspondingly, A Photon Shielding and Dosimetry "Phy-X/PSD" online software [30] was used to determine mass attenuation coefficients μ_m in a wide range of energy to meet reactor applications.

The effective atomic number (Z_{eff}) values of the prepared alloys were determined with the following equation:

$$Z_{eff} = \frac{\sigma_a}{\sigma_e} \quad \textbf{(10)}$$

Where σ_a and σ_e are the total atomic and electronic cross-sections, respectively [31, 32].

The equivalent atomic number(Z_{eq})values of the prepared alloys were obtained using the following equation:

$$Z_{eq} = \frac{Z_1(logR_2 - logR + Z_2(logR - logR_1)}{logR_2 - logR_1} \quad \textbf{(11)}$$

Where Z_1 and Z_2 are the constituent atomic numbers corresponding to R_1 and R_2 respectively, while R, is the ratio of Compton *MAC* to total *MAC* for the selected material at a particular energy [33].

Also, the exposure build-up factor *(EBF)* and energy absorption build-up factor *(EABF)* [34] were calculated by "Phy-X/PSD" software [30].

The experimental error due to the mass attenuation coefficients for gamma rays was calculated using the following equation [35]:

$$\Delta\mu_m = \frac{1}{x\rho}\sqrt{\left(\frac{\Delta I_0}{I_0}\right)^2 + \left(\frac{\Delta I_{(\gamma)}}{I_{(\gamma)}}\right)^2 + \left(\frac{\Delta x\rho}{x\rho}\right)^2\left(ln\left(\frac{I_0}{I_\gamma}\right)\right)^2} \quad \textbf{(12)}$$

Where ρ is the density of the alloy, $\Delta I_0, \Delta I_{(\gamma)}$ are the errors in the incident and transmitted intensities I_0, $I_{(\gamma)}$, respectively, and Δx is the error in thickness x of the sample.

2.5.2 Neutrons attenuation measurements

In the neutron attenuation investigation for the produced alloys, three neutron energies (slow neutrons, total slow neutrons, and neutrons with energies higher than 0.4 eV) were detected using a boron trifluoride (BF_3) detector. The total slow neutrons included both the primary slow neutrons radiated from the ^{241}Am- Be (α-n) source and those that slowed down in the examined alloys. In the slow neutron investigations, the neutron beam was being slowed down by a polyethylene block (7 cm) before the sample, and neutrons with energies below 0.4 eV were primary blocked by a cadmium sheet.

The neutron macroscopic cross section *(Σ)* was determined using the following equation [36, 37]:

$$I_{(n)} = I_0 e^{-\Sigma x} \quad \textbf{(13)}$$

Where, I_o and $I_{(n)}$ are the incident and transmitted neutron fluxes, respectively, and x is the thickness of the alloy.

The mean free path *MFP* was calculated using the following equation [38]:

$$MFP = \frac{1}{\Sigma} \quad \textbf{(14)}$$

The experimental error in the neutron macroscopic cross section *(ΔΣ)* [38] was calculated using the following equation:

$$\Delta\Sigma = \frac{1}{x}\sqrt{\left(\frac{\Delta I_0}{I_0}\right)^2 + \left(\frac{\Delta I_{(n)}}{I_{(n)}}\right)^2 + \left(\frac{\Delta x}{x}\right)^2\left(ln\left(\frac{I_0}{I_n}\right)\right)^2} \quad \textbf{(15)}$$

3. RESULTS AND DISCUSSION

3.1 Density and Molar Volume

Table 2 presents the experimental density ρ_{Exp}, calculated density ρ_{Cal}, and reference density ρ_{ReF} of (Bi-Pb) and (Bi-Pb-Sn) alloys. Figure 1 shows that ρ_{Exp} and ρ_{Cal} are approximately the same. Additionally, increasing Sn content reduces density, which agrees with [39]. In this investigation, the observed bulk density decreased from 10.55 g/cm^3 to 9.34 g/cm^3 with an increasing of Sn ratio at the expense of Pb, this may be due to that the density of Sn is less than that of Pb (ρ_{Sn}= 7.31 g/cm^3, ρ_{Pb}=11.35 g/cm^3) [10]. Therefore, the prepared (Bi-Pb-Sn) alloys exhibit outstanding natural coolant and heat transfer properties at a low-pressure.

Plevachuk et.al [40] studied the density of the 56Bi-44Pb alloy over the temperature range of 410–750 ºK, where the density is 10.08 g/cm^3. While the density for 46Bi -29Pb- 25Sn, over the temperature range of 375- 565 ºK is declining to 9.69 g/cm^3. Amer et.al [15] on the other hand studied adding 30 wt. % Cd to 55.5Bi- 44.5Pb, the density of which was 9.88 g/cm^3, while when substituted by 30 wt.% Sn to 50 Bi-20 Pb, the density decreased to 9.34 gm/cm^3. From these different studies, we concluded that adding Sn metal to (Bi-Pb) is a suitable choice for employing such alloys as coolants in fast fission and/or fusion nuclear reactors from the point of density view.

The LBE melts however with nearly no volume loss as one of its advances [10], this is related to the option of safe operation of the equipment during "freeze and unfreeze" LBE. The molar volume of LBE is 19.94 cm^3/mol [15]. As shown in Table 2 and Figure 1, the molar volume for the BL alloy in the current work is only 19.72 cm^3/mol, while once adding Sn on the expense of Pb, the value of molar volume is slightly reduced. It is important that the change in the rate of expansion on solidification in the reactor circuit is low. [10].

Table (2): Experimental density ρ_{Exp}, calculated density ρ_{Cal} , molar volume, and Porosity of (Bi-Pb) and (Bi-Pb-Sn) alloys.

Sample	ρ_{Cal} (g/cm^3)	ρ_{Exp} (g/cm^3)	ρ_{Ref} (g/cm^3) [39]	Molar Volume (cm^3/mole)	Porosity (%)
BL	10.55	10.55±0.05	-	19.72	0
BLSn1	9.90	9.85±0.05	9.69	19.69	0.51
BLSn2	9.74	9.70±0.05	9.53	19.63	0.47
BLSn3	9.54	9.46±0.05	9.32	19.65	0.80
BLSn4	9.34	9.31±0.05	-	19.49	0.27

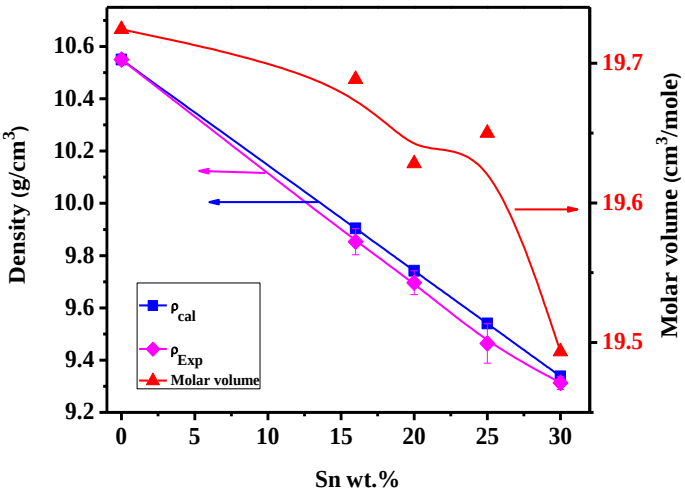

Fig. (1): Experimental density ρ_{Exp}, calculated density ρ_{cal} and molar volume as a function of Sn concentration wt. %. (curves have been drawn as a guide to the eye).

3.2 Differential thermal analysis (DTA)

Table 3 includes the melting points (T_m) of prepared alloys; it is shown that T_m of (Bi-Pb-Sn) alloys is lower by approximately 30 ºK compared to the BL alloy. Additionally, by increasing the Sn concentration in (Bi-Pb-Sn) alloys T_m remains almost fixed while it is lower than that of the BL alloy. The current results appear to be satisfactory in accordance with those of the other workers [39]. Reduced T_m for (Bi-Pb-Sn) alloys can affect the decrease the possible corrosion impact formed by Bi. It also enables the coolant to be used at lower temperatures, avoiding the risk of uncontrolled freezing. As a result, the lifetime of the reactor structural elements should be enhanced, and it is also ideal for cooling reactor outer blanket applications as well [15, 40]. This would simplify the operation and performance of (Bi-Pb-Sn) alloys as metal cooled reactors.

Table (3): Melting points, T_m, and contact angles on Al and St-37 substrates for (Bi-Pb) and (Bi-Pb-Sn) alloys.

	Melting points		Contact angles (degrees)	
Samples	T_m±1.5(°K)	T_m(°K) [39]	**Al**	**St-37**
BL	400	-	119	125
BLSn1	369	368	117	121
BLSn2	370	368-377	116	120
BLSn3	367	368-388	114	118
BLSn4	367	-	111	117

3.3 Wettability measurements

Among the most significant objectives in nuclear reactor design is to utilize transfer tubes and containers that are not reactive with coolant liquids, as well as avoid adding resistance to the ease of flow through the system and heat transfer lines [41]. That objective is typically defined by measuring the contact angle, CA, with various substrate materials.

Table 3 shows the contact angle values for (Bi-Pb) and (Bi-Pb-Sn) alloys with Al and St-37 substrates at an elevated temperature of 723 ºK. Also, Table 3 shows that the CA reduces when Sn is added to (Bi-Pb) with various substrates. Although this may be seemed as a drawback, however this is not the case where the prepared alloys are non-wetting because the CA is continued to be greater than 90º. Although, the maximum values of the contact angles were observed by means of St-37 substrates.

Surface tension on terms of CA is generally known to be proportional to the density of the corresponding alloy [42], as shown in Figure 2 Based on these findings; we concluded that St-37 is good candidates for use as vessels and pipes transporting the coolant around the reactor core. However, this result doesn't wipe up the possibility with using of the other alloy liquids as well. While employing the outside of the container blanket for thermal and nuclear radiation gamma and slow neutron shelters, including (Bi-Pb-Sn) alloys.

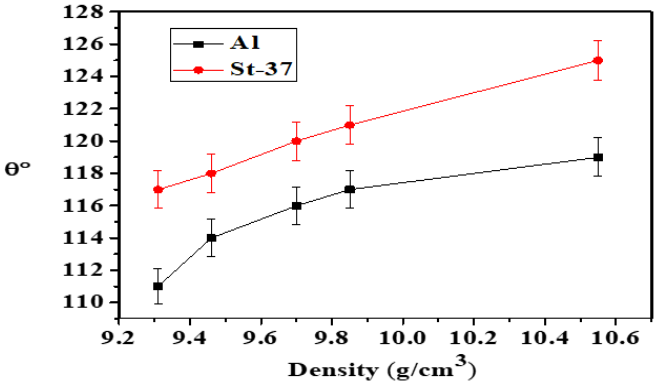

Fig. (2): The contact angle as function of the bulk density of the individual alloy. From Tables 2 and 3.

3.4 Nuclear measurements

3.4.1 Gamma-ray attenuation

Nine pronounced γ-ray emission peaks with energy ranges of 121.8 to 1407.24 keV were used to investigate the attenuation abilities of the prepared alloys. The *MAC* $\mu_m(cm^2/g)$ was calculated using Eqn. [8]. Figure 3 depicts a comparison of experimental values of $\mu_m(cm^2/g)$ in several examined alloys vs. gamma ray energies. Adding Sn to Bi and Pb has almost no effect on the value of $\mu_m(cm^2/g)$. This is due to the z dependency of gamma ray interactions with mostly lead and bismuth. Figure 4 indicates that experimental *MAC* show well with those computed by the "WinXCom" computer program (version 3.1). All these curves' behavior can be characterized by the Compton scattering process (CS), as the *MAC* gradually decreases with increasing γ-ray energy.

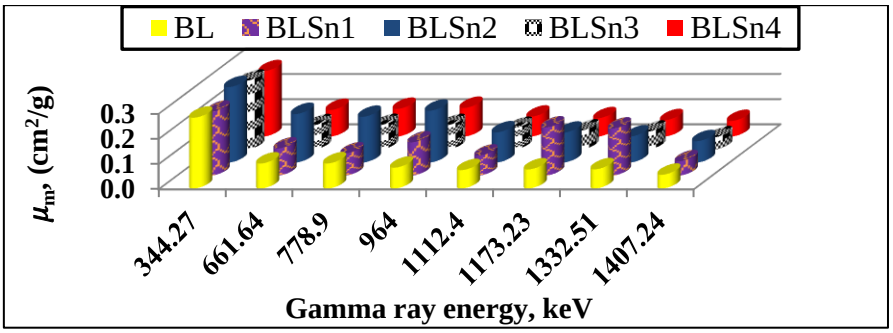

Fig. (3): Comparison between experimental mass attenuation coefficients at different energies for prepared alloys.

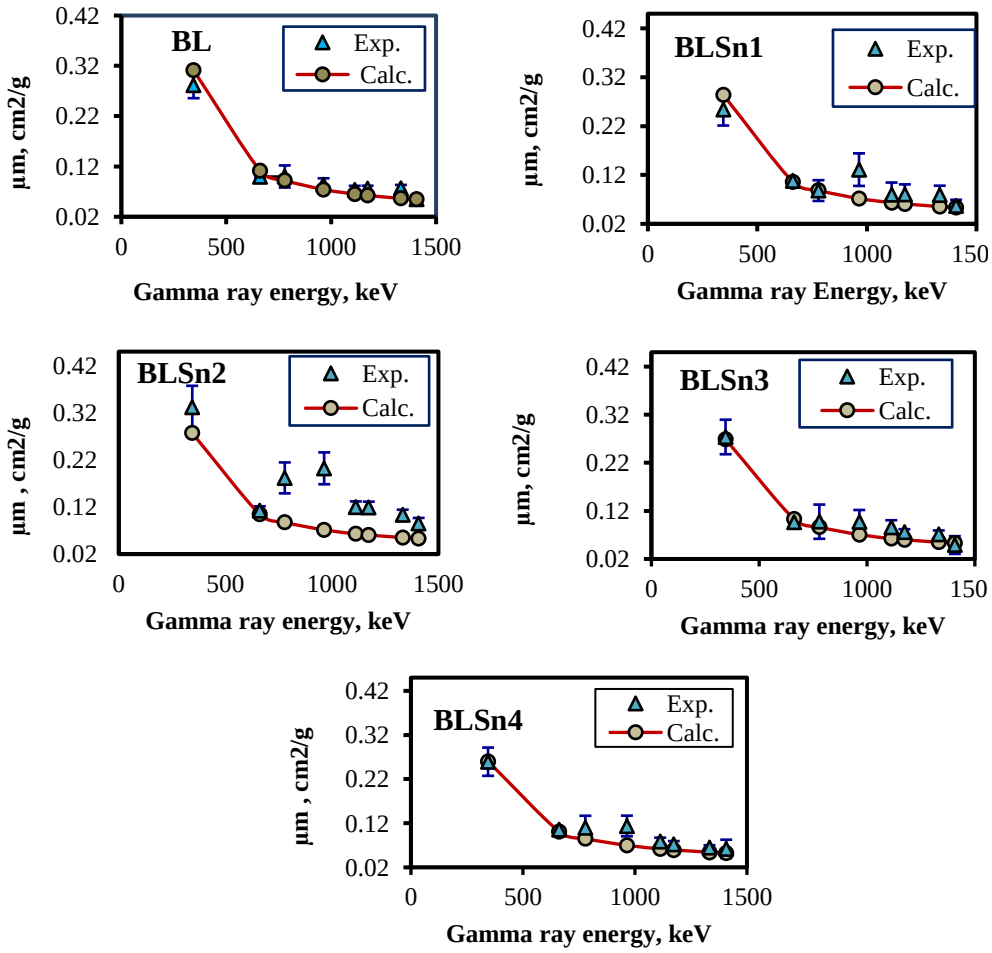

Fig. (4): Experimental and calculated mass attenuation coefficients by WinX-com computer program at different gamma ray energies for prepared alloys.

Figure 5 (a-d) shows the Comparison of μ_m, *HVL*, Z_{eff}, and *Zeq* against gamma –ray energies for (Bi-Pb) and (Bi-Pb-Sn) alloys, which were calculated by "Phy-X/PSD" software to cover high gamma ray energies (up to 10 MeV), as this sample was utilized as a coolant in fast fission and/or fusion nuclear reactors.

Figure 5(a) shows that: 1) Photoelectric absorption causes fast decreases in MAC values in the low energy zone. 2) The Pb and Bi elements' L and K absorption edges caused a major rise in MAC values. 3) The Compton scattering (CS) process causes the MAC to drop more slowly at medium energies. 4) After E≥ 1.022 MeV, MAC values began to increase due to pair production (PP) [31].

Figure 5(b) shows that: 1) the smallest values of half-value observed at energies between (0.015–0.1 MeV) 2) *HVL* values rapidly grow at energy 0.1 MeV due to secondary scattering enhancement with the impact of the (CS) process. 3) *HVL* quantities decrease beyond 3 MeV as a result of the (PP) process. 4) *HVL* is ~ 1.5 cm at energy equal to 10 MeV. The lower *HVL* values indicate better space efficiency. Because the thickness of this shield is minimal in comparison to other shields [43], the (Bi-Pb-Sn) cooled fast reactor will be quite small and can be applied to transportable and submarine reactors.

Figure 5(c) shows that the Z_{eff} value at low energies is higher than that at higher energies due to the photoelectric effect being dominant at low energies, whereas the influence due to scattering and (PP) processes is greater at higher energies [31, 44]. Figure 5(d) represents the comparison of Z_{eq} values against gamma –ray energies for (Bi-Pb) and (Bi-Pb-Sn) alloys, demonstrating that Z_{eq} reaches its greatest value in the region where (CS) process is common.

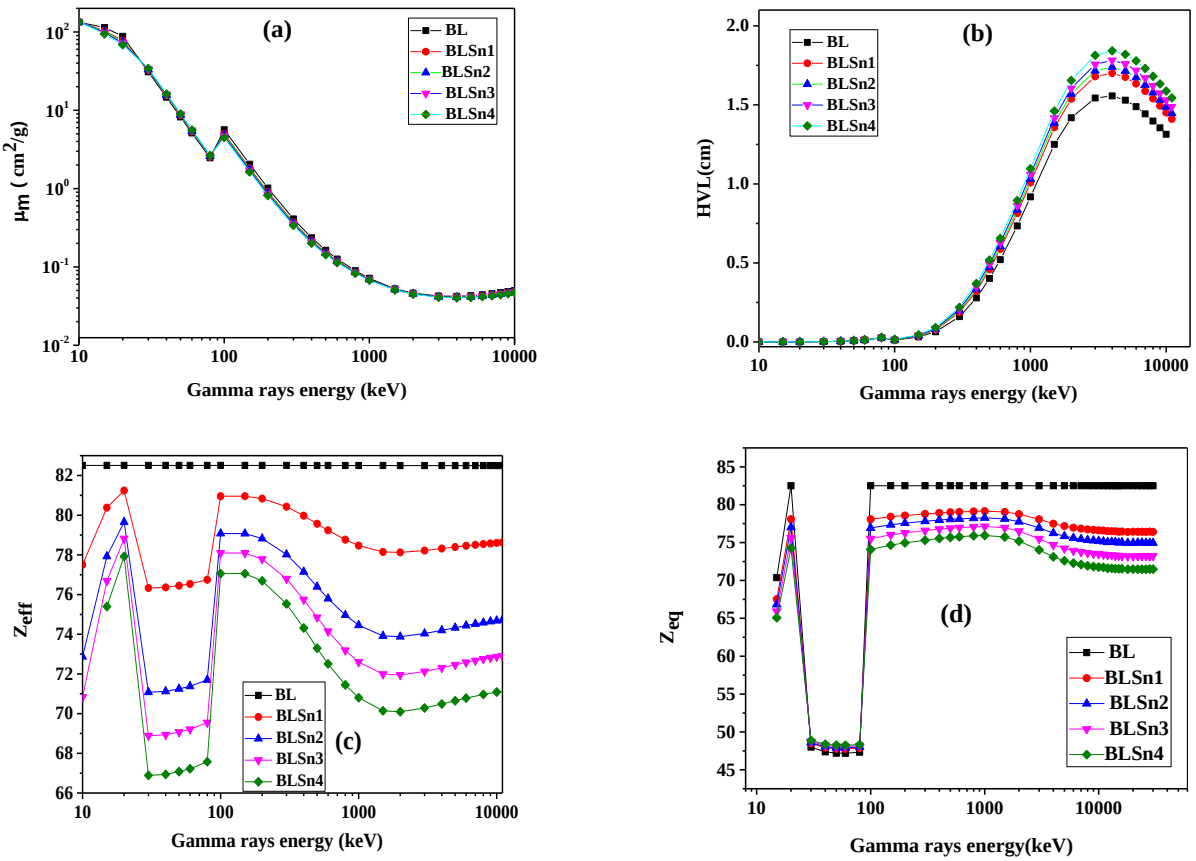

Fig. (5): Comparison of (a)μ_m, (b) HVL, (c) Z_{eff}, and (d) Z_{eq} against gamma –ray energies for (Bi-Pb) and (Bi-Pb-Sn) alloys.

"Phy-X/PSD" software was used to calculate energy absorption build-up factors (*EABF)* and energy exposure build-up factors (*EBF*) for (Bi-Pb) and (Bi-Pb-Sn) alloys in the gamma –rays energy range (0.03-10 MeV). Figures 6 and 7 show the comparison of EBF and *EABF* against gamma –ray energies for (Bi-Pb) and (Bi-Pb-Sn) alloys. It was observed that, there are very steep peaks about 0.1 MeV, which correspond to the Pb and Bi elements' L and K absorption edges. The high *Z* values of the essential elements increase the probability of photoelectric absorption (PEA) collision, leading to gamma accumulation. The (*EBF)* and (*EABF)* values of BL alloys are considerably higher than those that contain Sn.

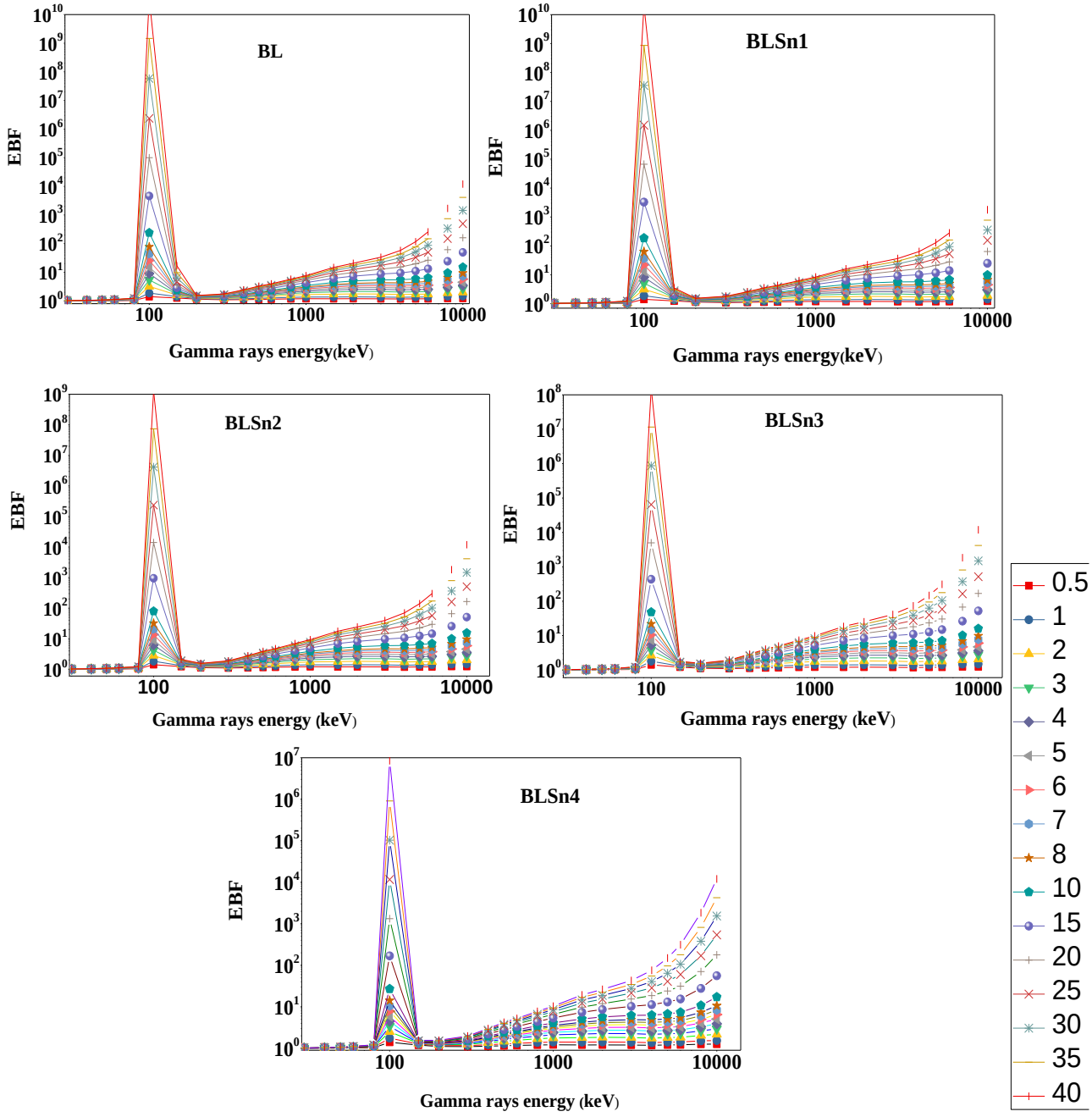

Fig. (6): Comparison of EBF against gamma –ray energies for (Bi-Pb) and (Bi-Pb-Sn) alloys.

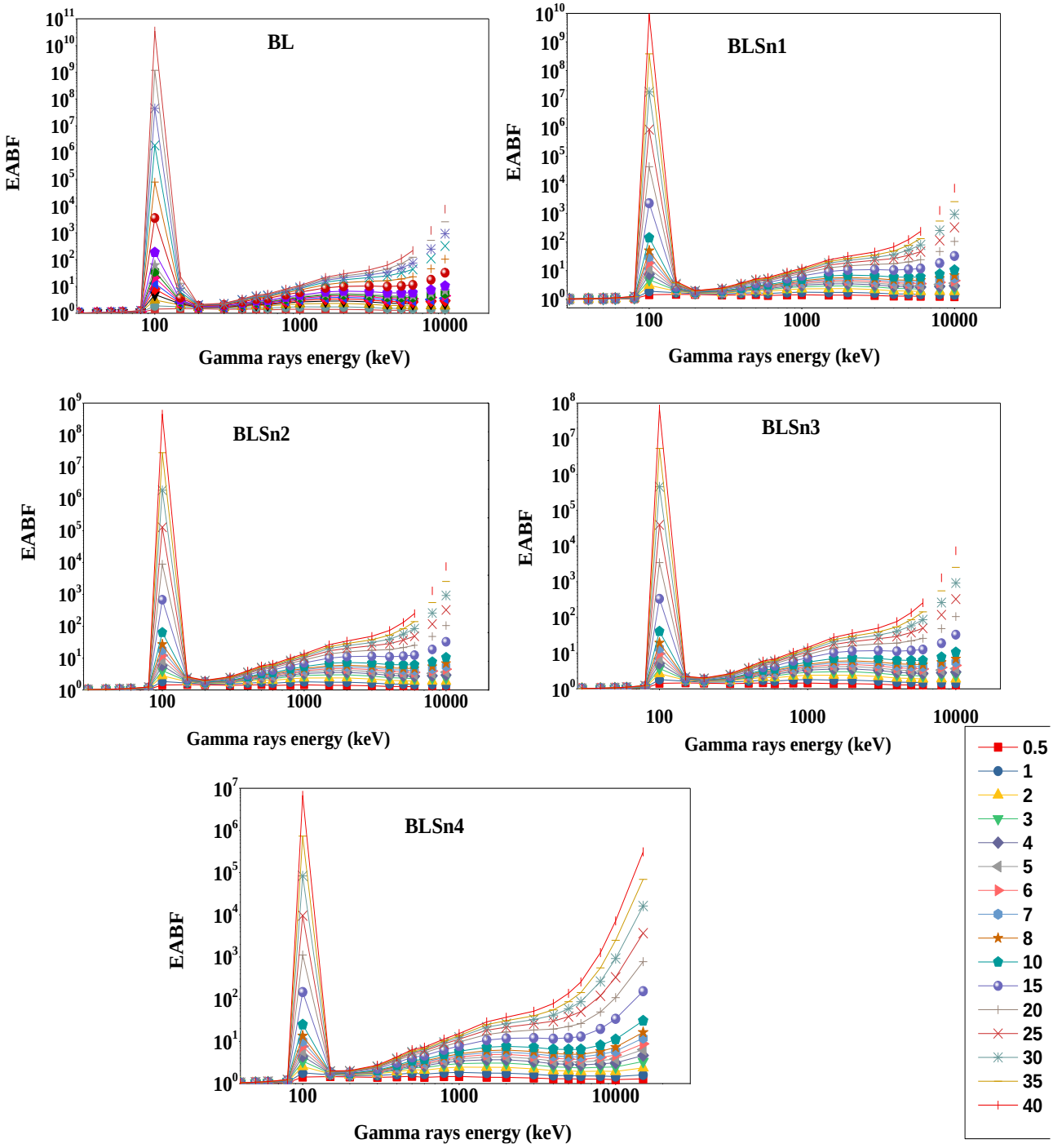

Fig. (7): Comparison of EABF against gamma –ray energies for (Bi-Pb) and (Bi-Pb-Sn) alloys.

3.4.2 Neutrons attenuation measurements

Boron trifluoride BF_3 neutron detector tube and three neutron energies regions (slow neutrons, total slow neutrons, and neutrons with energies > 0.4 eV) were utilized to deduce the macroscopic cross-section (Σ_S, Σ_T, and Σ_E *>0.4eV* respectively) in the prepared five sample concentrations. From Figure 8(a), there is a slight increase in the value of Σ_S with raising the tin weight percentage up to 30 wt.%; unless 25 wt.%, there is a slight decrease in the opposite value of Σ_S This act may be explained by considering that there is no obvious effect of both Bi, Pb, and Sn nuclei on slow neutron macroscopic cross-section (slow neutrons are less probable to interact with Pb and Bi as (n,γ) reactions) [17] because the main probable interaction of these nuclei is with fast neutrons by inelastic scattering. While in Figure 8(b) and (c), there is a significant increase in the Σ_T and Σ_E *>0.4eV* values by increasing Sn wt.% in

(Bi-Pb-Sn) alloys, except for 25 wt.% of Sn. Which may be attributed to a high fast neutron interaction probability with Bi, Pb, and Sn nuclei as (n, 2n) and (n, n\) interactions of fast neutrons [45]. Moreover, the negative behavior of neutron macroscopic cross-sections of Sn with a percentage concentration of 25 wt.% in all used neutron energy regions is because of its high porosity content among other percentages of Sn, as is clear in Table 2. The measured *MFP* (cm) values of prepared alloys are represented in Table 4 and Figure 9.

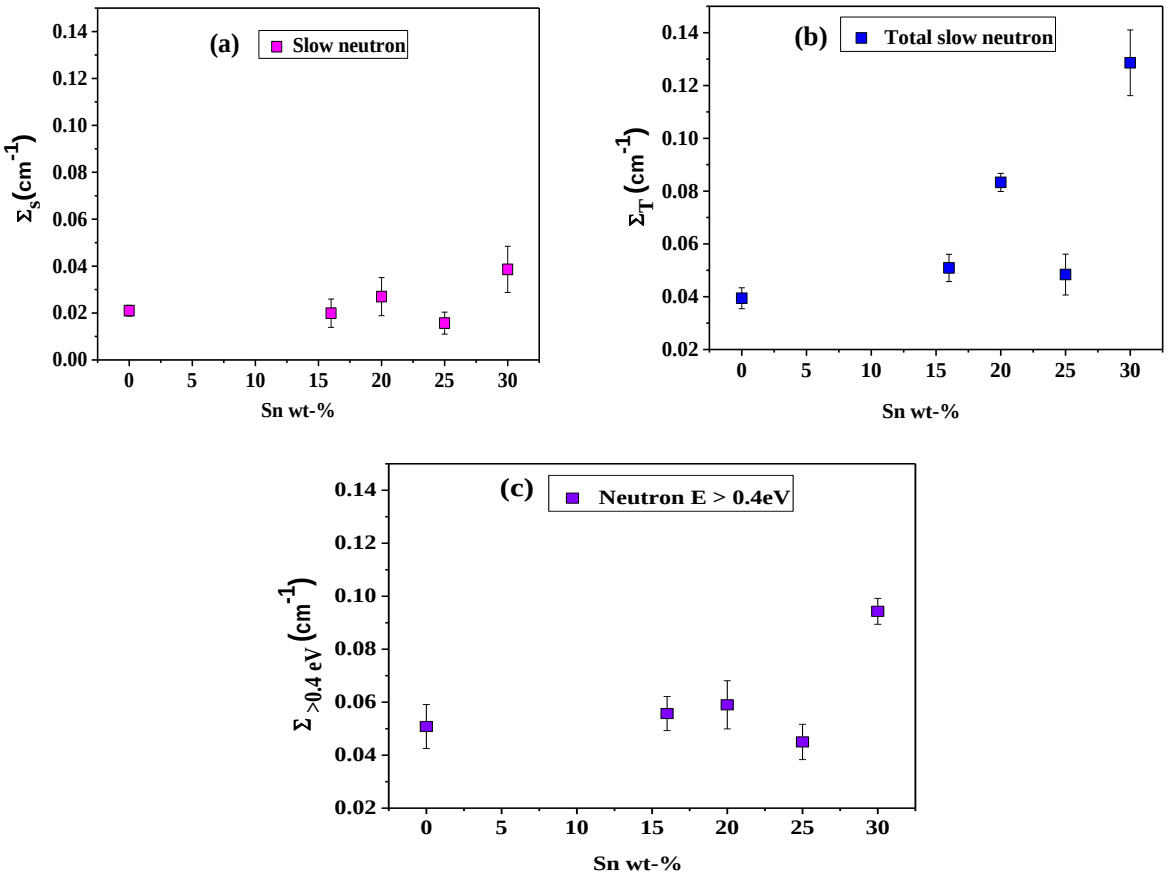

Fig. (8): The Σ, (cm^{-1}) values of (Bi-Pb) and (Bi-Pb-Sn) alloys with different neutron energies.

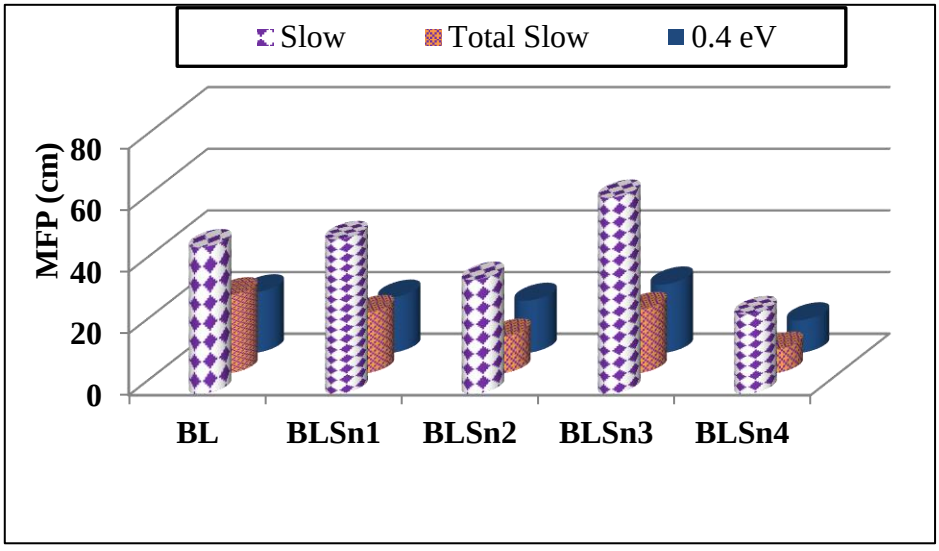

Fig. (9). Mean free paths (MFP) of (Bi-Pb) and (Bi-Pb-Sn) alloys with different neutron energies.

Table (4): The Σ, (cm^{-1}), and *MFP* (cm) of (Bi-Pb) and (Bi-Pb-Sn) alloys with different neutron energies.

Sample	Energy	Σ, (cm-1)± ΔΣ	MFP (cm)
BL	Slow	0.0210±0.0023	47.619
	Total Slow	0.0394±0.0040	25.380
	> 0.4 eV	0.0508±0.0083	19.685
BLSn1	Slow	0.0199±0.0060	50.251
	Total Slow	0.0509±0.0052	19.646
	> 0.4 eV	0.0557±0.0065	17.953
BLSn2	Slow	0.0270±0.0081	37.037
	Total Slow	0.0833±0.0034	12.005
	> 0.4 eV	0.0590±0.0091	16.949
BLSn3	Slow	0.0157±0.0047	63.694
	Total Slow	0.0484±0.0077	20.661
	> 0.4 eV	0.0450±0.0067	22.222
BLSn4	Slow	0.0386±0.0098	25.907
	Total Slow	0.1286±0.0125	07.776
	> 0.4 eV	0.0943±0.0049	10.604

4. CONCLUSIONS

A set of Bi-Pb-Sn alloys was fabricated and prepared to measure their thermal properties as well as their nuclear radiation characteristics against gamma rays and neutron particles with a view to being applied as a coolant in fast fission and/or fusion nuclear reactors. The bulk density of (Bi-Pb-Sn) alloys decreased as the Sn concentration increased; there is no need for high pumping power for cooling circulation. The T_m decreased with the replacement of Sn at the expense of Pb, and this works to reduce corrosion resulting from Bi and avoid the risk of uncontrolled freezing. The liquid alloys are non-wetting with different substrates (Al and St-37).

The experimental values of mass attenuation coefficients of gamma-rays in the produced alloys correlate well with those estimated using the "WinXCom" computer program and "Phy-X/PSD" software. Adding Sn to Bi and Pb does not significantly affect the mass absorption coefficient μ_m (cm^2/g). Based on the neutron macroscopic cross section values Σ, (cm^{-1}), it is better to use BLSn2 alloy in the primary loop of the LMFR because the absorption of fast neutrons used in the breeder reactor is lower, while BLSn4 alloy is a good choice to use in the secondary loop due to the large absorption of fast neutrons to prevent radioactive contamination. In the end, the addition of Sn to Bi and Pb improves physical as well as attenuation properties. Based on this conclusion we propose that the liquid metal alloys of (Bi-Pb-Sn) can be utilized as coolant for nuclear reactors.

REFERENCES

[1] Samue D. (2009) Molten Salt Coolants for High Temperature Reactors, Intern, NENP-TDS/INPRO, IAEA.

[2] Frazer D., Stergar E., Cionea C., Hosemann P. (2014), Liquid metal as a heat transport fluid for thermal solar power applications, Energy Procedia, 49, 627–636. https://doi.org/10.1016/j.egypro.2014.03.068

[3] Kunquan M.A., Liu J. (2007) Liquid metal cooling in thermal management of computer chips, J. Front. Energy Power Eng. China, 1 [4], 384-402. https://doi.org/10.1007/s11708-007-0057-3

[4] OECD/NEA Nuclear Science Committee. (2007) Handbook on Lead-bismuth Eutectic Alloy and Lead Properties, Materials Compatibility, Thermal Hydraulics and Technologies, Nuclear Energy Agency.,

[5] Marques R.V.A., Velasquez C.E., Pereira C., Barros G.P., Veloso M.A.F., Costa A.L. (2017) Liquid Metal Coolants for Fusion-Fission Hybrid System – A Neutronic Analysis, International Nuclear Atlantic Conference, Belo Horizonte, MG, Brazil.

[6] You J.H., Mazzone G., Visca E. (2022) Divertor of the European DEMO: Engineering and technologies for power exhaust, Fusion Eng. Des, 175, 113010. https://doi.org/10.1016/j.fusengdes.2022.113010

[7] Deng Y., Jiang Y., Liu J. (2021) Liquid metal technology in solar power generation - Basics and applications, Sol. Energy Mater, Sol. Cells, 222, 110925. https://doi.org/10.1016/j.solmat.2020.110925

[8] Li Y., Zhang S., Ding Q., Feng D., Qin B., Hu L. (2018) Liquid metal as novel lubricant in a wide temperature range from −10 to 800 °C, Mater. Lett, 215, 140–143. https://doi.org/10.1016/j.matlet.2017.12.091

[9] Abderrhaim H.A., Baeten P., Didier J. D. B, Heyse J., Schuurmans P., Wagemans J . M. (2110) Multipurpose hybrid research reactor for high-tech applications, Nucl. Phys. News, 20(1), 24-28. https://doi.org/10.1080/10506890903178913

[10] Bogoslovskaya G.P. (2002) Comparative Assessment of Thermophysical and Thermohydraulic Characteristics of Lead, Lead-Bismuth and Sodium Coolants for Fast Reactors, IAEA TECDOC-1289, IAEA, Vienna June.

[11] El-Genk M. S., Tournier J.M. P. (2011) Uses of liquid-metal and water heat pipes in space reactor power systems, Front. Heat Pipes, 2 (1), 013002. https://doi.org/10.5098/fhp.v2.1.3002

[12] Weeks J.R. (1971) Lead, Bismuth, Tin and Their Alloys as Nuclear Coolants, Nucl. Eng. Des, 15, 363-372. https://doi.org/10.1016/0029-5493(71)90075-6

[13] Qian L. (1992) Proc. of Int. Conf. on Advanced Nuclear Power Plants, Tokyo, Japan.

[14] Toshinsky G. I., Dedul A. V., Komlev O. G., Kondaurov A. V , Petrochenko V. V. (2020) Lead-Bismuth and Lead as Coolants for Fast Reactors, World. J. of Nuc. Sci. Technol, 10, 65-75. https://doi.org/10.4236/wjnst.2020.102007

[15] Amer T.Z., Saleh S. E., El Shazly R.M., Gomaa N.S. Bahgat A.A. J. (2019) Study of the physical and nuclear properties of liquid PbBiCd alloy coolant in nuclear fast reactor, J. Nucl. Mater, 522, 226-235. https://doi.org/10.1016/j.jnucmat.2019.05.006

[16] Dahy S., Amer T. Z., El Shazly R. M., Gomaa N. S., Bahga A. A. (2023) Elucidating of the influence of tin and cadmium in the Bi–Pb alloy on its thermal and nuclear properties as a coolant in fast neutron reactors. Radiat. Eff. Defects Solids, 178, 1282-1300. https://doi.org/10.1080/10420150.2023.2245100

[17] Can, L. (2006) Analysis of Coolant Options for Advanced Metal Cooled Nuclear Reactors, Thesis, Naval Postgraduate School, California.

[18] Bahgat A.A., El-Bahay M.M., El-Mossalamy M.E., Mahdy M. (2005) Creep Behavior of the Eutectic Sn- 9 wt.% Zn Alloy, J. Pure & Appl. Phy, 1, 55-69. https://www.researchgate.net/publication/300103168

[19] Bahgat A.A., El Bahnasawy H. Differential Thermal Analysis “DTA” https://doi.org/10.13140/RG.2.2.26946.45767/1

[20] Rusu D., Ardelean I. (2008) Structural studies of Fe2O3–Bi2O3–CdO glass system. Mater. Res. Bull. 43, 1724-1730. https://doi.org/10.1016/j.materresbull.2007.07.016

[21] Awasthi A., Bhatt Y. J., Garg S. P. (1996) Measurement of contact angle in systems involving liquid metals, Meas. Sci. Technol, 7, 753–757. https://doi.org/10.1088/0957-0233/7/5/005

[22] Zhang Yi. (2016) Static and Dynamic Behaviour of Inter-granular Liquid Bridges: Hysteresis of Contact Angle and Capillary Forces.

[23] Yuehua Y., Lee T.R. (2013) Contact Angle and Wetting Properties, Eds. Bracco G., Holst. Surface Science Techniques, Springer Series in Surface Sciences, Springer-Verlag Berlin Heidelberg. https://doi.org/10.1007/978-3-642-34243-1_1

[24] Veazey S. D., Roe W. C (1972) Review: Density measurements in liquid metals and liquid binary alloy systems --A survey, J. Mater. Sci., 7, 445-466. https://doi.org/10.1007/BF00553769

[25] Creutz E., Jupnik H., Wigner E. P (1955) Effect of Temperature on Total Resonance Absorption of Neutrons by spheres of uranium oxide, J. Appl. Phys. 26(3), 276. https://doi.org/10.1063/1.1721977

[26] Stankus S.V., Khairulin R.A., Mozgovoy A.G., Roshchupkin V.V, Pokrasin M.A (2008) The density and thermal expansion of eutectic alloys of lead with bismuth and lithium in condensed state, J. Phys. Conf. Ser., 98, 062017. https://doi:10.1088/1742-6596/98/6/062017

[27] Lamarsh J.R. (2001) Baratta A.J. Introduction to Nuclear Engineering, 3ed, Prentice- Hall, Inc., New Jersey, pp. 548

[28] XCOM: Photon Cross Sections Database, https://physics.nist.gov/PhysRefData/Xcom/html/xcom1.html

[29] El Shazly R.M., Sadawy M.M. (2017) Effect of slag as a fine aggregate on mechanical, corrosion, and nuclear attenuation properties of concrete, Int. J. Sci. Eng. Res, 5, 243-250. https://www.researchgate.net/publication/324331069

[30] Phy-X / PSD: Photon Shielding and Dosimetry, https://phy-x.net/PSD

[31] Almisned G., Tekin H.O., Kavaz E., Bilal G., Issa S.A.M., Zakaly H.M.H., Ene A. (2021) Gamma, Fast Neutron, Proton, and Alpha Shielding Properties of Borate Glasses, Appl. Sci, 11, 6837. https://doi.org/10.3390/app11156837

[32] Han I., Demir L. (2009) Determination of mass attenuation coefficients, effective atomic and electron numbers for Cr, Fe and Ni alloys at different energies, Nucl. Instrum. Methods Phys. Res. Sect. B Beam Interact, Mater. Atoms, 267, 3–8. https://doi.org/10.1016/j.nimb.2008.10.004

[33] ANSI/ANS-6.4.3, (1991) Gamma Ray Attenuation Coefficient and Buildup Factors for Engineering Materials, American Nuclear Society La Grange Park, IL.

[34] Şakar E., Özpolat O. F., Alım B., Sayyed M.I., KurudirekM. (2020) Phy-X / PSD: Development of a user-friendly online software for calculation of parameters relevant to radiation shielding and dosimetry. Radiat, Phys. Chem, 166, 108496. https://doi.org/10.1016/j.radphyschem.2019.108496

[35] Saeed A., El bashar Y.H., El Shazly R.M. (2016) Optical properties of high-density barium borate glass for gamma ray shielding applications, Opt. Quantum Electron, 48 (1), 1-10. https://doi.org/10.1007/s11082-015-0274-3

[36] Lilley J.S. (2002) Nuclear physics principle and applications, John Wiley & Sons, Ltd.,

[37] Sayyed M.I., Qashou S.I., Khattari Z.Y. (2017) Radiation shielding competence of newly developed TeO2-WO3 glasses, J. Alloys Compd, 696, 632–638. https://doi.org/10.1016/j.jallcom.2016.11.160

[38] Taylor, J.R. (1982) An Introduction to error analysis the study of uncertainties in physical measurements, 2nd edn., Sausalito, California, University science books.

[39] More Industrial Alloys, https://www.aimalloys.com/sites/default/files/other_industrial_alloy_chart_sept14.pdf

[40] Plevachuk Y., Sklyarchuk V., Gebeth G. Eckert S., Novakovic R. (2011) Surface tension and density of liquid Bi-Pb, Bi-Sn and Bi-Pb-Sn eutectic alloys, Surface Science 605,1034–1042. https://doi.org/10.1016/j.susc.2011.02.026

[41] Quere, D. (2008) Wetting and roughness, Annu. Rev, Mater. Res, 38, 71-99. https://doi.org/10.1146/annurev.matsci.38.060407.132434

[42] Alchagirov B.B., Shamparov T.M., Mozgovoi A.G. (2003) Experimental investigation of the density of molten lead-bismuth eutectic. High Temp, 41 [2], 210-215. https://doi.org/10.1023/A:1023325601527

[43] Awadallah M. I., Imran M.M.A. (2007) Experimental investigation of γ-ray attenuation in Jordanian building materials using HPGe-spectrometer, J. Environ. Radioact, 94, 129-136. https://doi.org/10.1016/j.jenvrad.2006.12.015

[44] Oto B., Oto G., Madak Z., Kavaz E. (2019) The interaction of gamma radiation with drugs used in cholinergic medications, Int. J.Radiat. Biol, 96, 236–244. https://doi.org/ 10.1080/09553002.2020.1683640

[45] IAEA. (1974) Handbook On Nuclear Activation Cross-Sections, VIENNA.